Early View publication on wileyonlinelibrary.com
(issue and page numbers not yet assigned;
citable using Digital Object Identifier – **DOI**)

Phys. Status Solidi C, 1–5 (2011) / **DOI** 10.1002/pssc.201083991

physica status solidi c
www.pss-c.com
current topics in solid state physics

Cross sectional evaluation of boron doping and defect distribution in homoepitaxial diamond layers

Daniel Araújo*,1, M. A. Paz Alegre[1], Antonio J. García[1], M. Pilar Villar[1], Etienne Bustarret[2], Philipp Achatz[2], Pierre N. Volpe[2], and Franck Omnès[2]

[1] Universidad de Cádiz, Dpto. Ciencia de los Materiales, 11510 Puerto Real, Cádiz, Spain
[2] Institut Néel, CNRS and UJF, Av. des Martyrs 25, 38041Grenoble, France

Received 5 July 2010, revised 17 September 2010, accepted 8 November 2010
Published online ZZZ

Keywords homoepitaxial diamond, boron-doped, TEM, HAADF, CL

* Corresponding author: e-mail daniel.araujo@uca.es, Phone: +00 34 956 016 427, Fax: +00 34 956 016 288

In some diamond-based semiconducting devices, large variations of doping level are required over short distances. Tools to determine doping level and defects distribution should therefore be developed. The present contribution shows the capabilities of electron microscopy in this field. Focused ion beam (FIB-dual beam) cross section preparations allowed evaluating doping level in highly boron doped sample with doping transition down to some nm by diffraction contrast mode of transmission electron microscopy (CTEM) and by high angle annular dark field mode of scanning transmission electron microscopy (HAADF-STEM). The sensibility of the latter is around 10^{19}cm^{-3} and, thus, cathodoluminescence (CL) is required for lower doping levels. Cross sectional analysis on FIB prepared lamella allowed to separate the epilayer behaviour from that of the substrate. Mid-gap centers involving boron, hydrogen and, for some peaks, also nitrogen are revealed. sp^2 bonds are also present in the grown epilayer. These transitions make difficult the observation of excitonic recombinations in the cross section configuration.

© 2011 WILEY-VCH Verlag GmbH & Co. KGaA, Weinheim

1 Introduction Since several decades, many groups worldwide have been actively investigating diamond material to obtain semiconducting devices. Indeed, its intrinsic properties make it very attractive for such purpose. Its large bandgap (5.49 eV) allows insulating, semiconducting or metallic epilayers, its high breakdown field (>10 000 V) allows to fabricate records Schottky diodes without breakdown up to 7500 V and its highest hole mobility (3800 cm^2/V s) among the semiconducting materials and very competitive electron mobility (4500 cm^2/V·s) motivate the fabrication of high frequency devices. Besides, the very large thermal conductivity (22 W/cm·K, around five times that of Cu or SiC) makes it very attractive for power devices [1].

According to such considerations, Balmer *et al.* [2] proposed the implementation of δ-doped epitaxial structure to develop MESFET transistor devices oriented to high velocity and high power applications. The idea is to yield holes in an undoped diamond channel using a δ-doped epilayer. Then, if the thickness of such a layer is below 5 nm, the wave function of the holes floods around and stands mainly in the undoped material taking advantage of its high hole mobility characteristics.

However, in practice, the growth of such thin layer is not straightforward as doping level up to 10^{21} cm^{-3} should be reached to deliver sufficient holes to the channel. Kohn *et al.* [1] achieved doping transitions above 25 nm, which is too large. The experimental methodology generally used for such measurements is the secondary ion mass spectroscopy (SIMS), which delivers depth (z-axis) doping profiles (over 50 to 200 µm-sized square spots). Thus, no submicrometer in-plane (x-y axis) information is available. Lateral doping variation can thus induce artefacts in the SIMS profile. In the present paper, alternative techniques using cross sectional focused ion beam (FIB) prepared lamella, followed by electron microscopy observation, is presented. In addition, crystalline defects which may also affect carrier mobility may be detected at the same time using such a methodology.

2 Experimental Two samples were grown by microwave plasma chemical vapour deposition (MPCVD) in a

© 2011 WILEY-VCH Verlag GmbH & Co. KGaA, Weinheim

vertical silica tube reactor as described elsewhere [3] on (100) oriented diamond substrates. One was grown with a very high boron doping while the second with a very low doping, in order to investigate the large range methods to be used to assess doping and defects. The first sample A (PA14) consists in a 700 nm thick epilayer with a very high boron doping of 10^{21} cm^{-3} determined by SIMS. This epilayer was grown on a HPHT type Ib diamond substrate (optimized growth conditions used are a temperature of 830 ºC, a pressure of 30 Torr and a CH_4/H_2 methane concentration of 4% for 40 min). The second sample B (PNV42) consists of a 2 µm thick epilayer grown on a CVD (E6) optical grade quality substrate (optimized growth conditions used are a temperature of 910 ºC, a pressure of 50torr and a CH_4/H_2 methane concentration of 1% for 3 hours). The doping level is estimated around 10^{16} cm^{-3} by cathodoluminescence spectroscopy (CL) following the methodology proposed by Kawarada *et al.* [4] and Deneuville *et al*. [5].

Samples are prepared by the FIB-assisted lift off technique to obtain cross section specimens. The thickness is around 80nm for the TEM lamella and around 500nm for the CL cross section investigations.

TEM studies are carried out for this material. Diffraction contrast (DC) measurements are performed on a Jeol 1200EX, operating at 120 keV. HAADF-STEM experiments are carried out on a Jeol 2010F (high resolution objective lens with FEG gun) operating at 200 keV. CL measurements are performed on a FEI Quanta200 at 10 keV.

3 Results and discussion To evaluate boron doping, different electron microscopy related techniques are here employed. On one side, variations in recorded intensity of diffraction contrast and in high angle annular dark field, both techniques of transmission electron microscopy here performed on cross section foils, can give information about the dopant level. On the other hand, from cathodoluminescence, the relative intensities of the CL exciton bound to boron peak (BE_{TO}) respect to that of the free exciton (FE_{TO}) allow to determine the doping level, while monochromatic CL maps at the BE_{TO} energy inform on the distribution of incorporated boron (i.e. active boron).

3.1 B doping evaluation by TEM related techniques First, diffraction contrast is considered, as the recorded intensity is related, in two beams conditions, both to thickness and to extinction distance [6]. Figure 1 shows two micrographs in dark field (DF) mode using 111 and 004 reflections, where the undoped-doped transition contrast is evident. No dislocations have been revealed in this sample, neither at the substrate-epilayer interface nor into the grown layer.

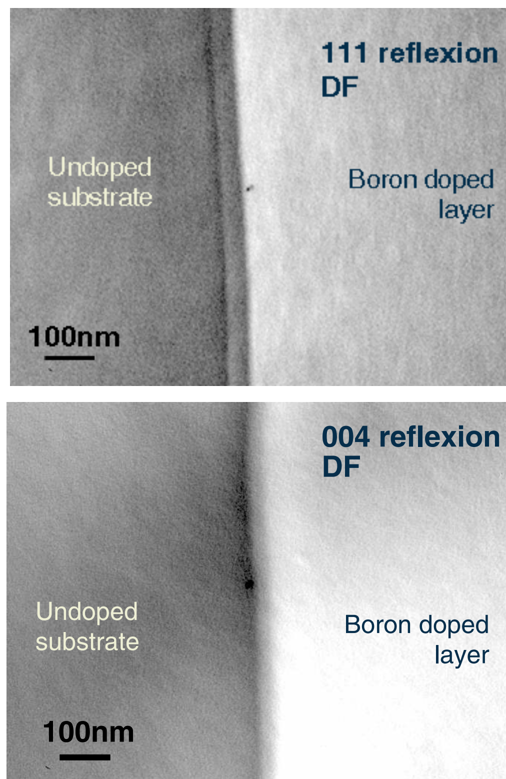

Figure 1 Diffraction contrast micrographs recorded on sample A using 111 (up) and 004 (down) reflections in dark field (DF) conditions. The undoped substrate and buffer layer are shown to be darker than the boron doped epilayer.

In two beams conditions, the intensity recorded follows the expression [7]:

$$\left|\Phi_g\right|^2 = \sin^2\left(\frac{\pi t}{\xi_g}\right) \qquad (1)$$

where ξ_g is the extinction distance for the reflection g and t is the thickness of the sample. Considering the definition of the extinction distance, Eq. (1) can be rewritten as follows:

$$I_{hkl} = \sin^2\left[\frac{\lambda 8 f_{eff} z}{V_c \cos\theta_B}\right] = \sin^2\left[C_{hkl} f_{eff} z\right] \qquad (2)$$

being λ the electron wavelength, V_C the unit cell volume, θ_B the Bragg angle, z the foil thickness and f_{eff} the effective atomic scattering factor, which varies with the boron content as follows:

$$f_{eff} = x \cdot f_B + (1-x) \cdot f_C \qquad (3)$$

where f_B and f_C are the atomic scattering factors of boron and carbon, respectively.

© 2011 WILEY-VCH Verlag GmbH & Co. KGaA, Weinheim

Obviously, tilting to reach the expected reflection affects to the effective thickness crossed by the electron beam. Therefore, contrasts can be inverted depending on the thickness or on the diffracted beam, *g*, used to record the micrograph (extinction distance changes with *g*). As ξ depends directly on the structure factor and thus on the atomic scattering factor and, in consequence, on the atomic number *Z*, a contrast is observed when boron is incorporated to the diamond crystal. When representing the intensity recorded under a certain reflection versus the thickness, varying both the thickness and the boron content to fit curves with experimental contrasts, the effect of boron incorporation into the diamond lattice can be appreciated, as Fig. 2 shows.

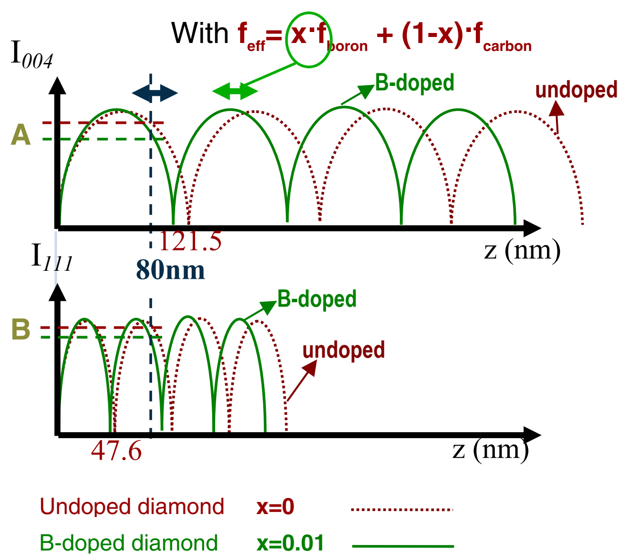

Figure 2 Representation of the intensity for 004 (up) and 111 (down) reflections versus foil thickness crossed by the electron beam from 004 and 111 DF micrographs, respectively. Depending of the thickness, contrast can be completely inverted. Dashed line corresponds to the non-doped substrate contrast, while continuous line corresponds to the boron-doped diamond epilayer. A and B indicate the difference in contrast between substrate and epilayer recorded in the DC micrographs (see Fig. 1).

Using two different reflections exactly in the same conditions of brightness and contrast in the recording system, thickness and ξ can be determined, what allows to know the doping level. In this case, a foil thickness of around 80 bnm and a boron content of the layer of around 10^{21} cm^{-3} is here estimated.

HAADF-STEM measurements are obtained from the same sample, in order to also validate this methodoly as suitable to evaluate de boron content in diamond homoepitaxial layers. In this technique, the signal collected at high angles results from incoherent scattering with thermally excited atoms of the analyzed sample. These high angle scattered electrons do not contribute to the Bragg diffraction (BS), i.e. elastic electrons intensity is reduced by the effect of the temperature as electron are diffused at higher angles, and are labeled “thermally diffuse scattering (TDS)” [8].

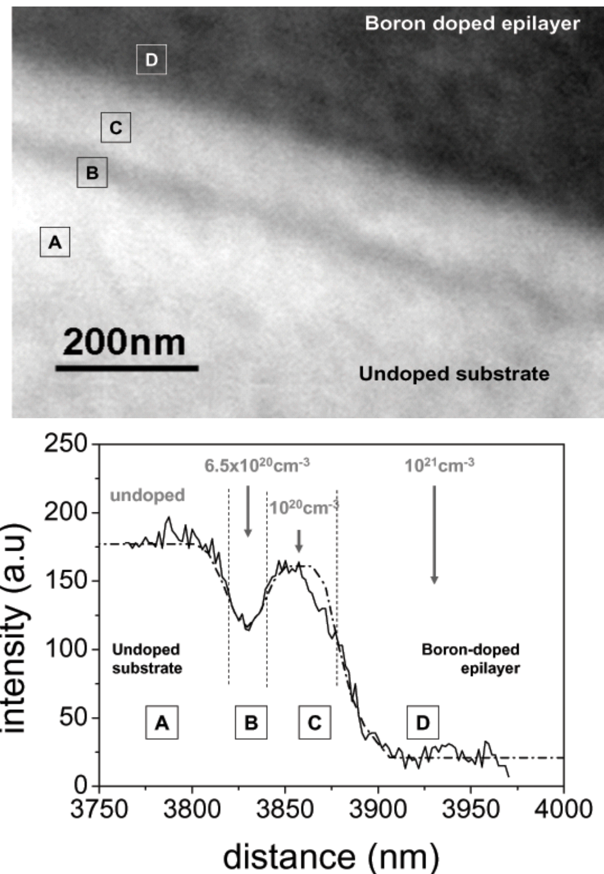

Figure 3 Experimental and simulated HAADF intensity profiles of the upper micrograph, once transformed to direct contrast, showing the different regions along the profile, as marked in the micrograh labelling from A to D. Quantification resulting from simulations corroborate DC results.

HAADF is also named Z-contrast, as the amplitude is linear with thickness and intensity depends on Z^2. One of the main advantages of HAADF measurements versus DC ones is that tilting effects are completely eliminated, since HAADF contrast do not require tilting of sample in the microscope. On the other hand, a nanometric, even atomic, resolution can be reached in HAADF experiments. In this sense, a modulation in the composition of the buffer layer is detected, estimating the thickness of this buffer layer in around 50nm.

Numerical simulations of the HAADF intensity along a profile across the substrate/boron-doped epilayer interface allow quantifying the dopant content. Figure 3 shows the experimental and simulated HAADF intensities, with very good agreement between them. Details of how simulations are carried out have been published elsewhere [9]. As can

© 2011 WILEY-VCH Verlag GmbH & Co. KGaA, Weinheim

be seen, HAADF results corroborate DC ones, with a much better spatial resolution.

3.2 CL spectroscopy When doping is below the 10^{19}cm^{-3} scale, CTEM and HAADF analysis cannot be carried out as sensitivity of the techniques is not sufficient. Then, CL should be used.

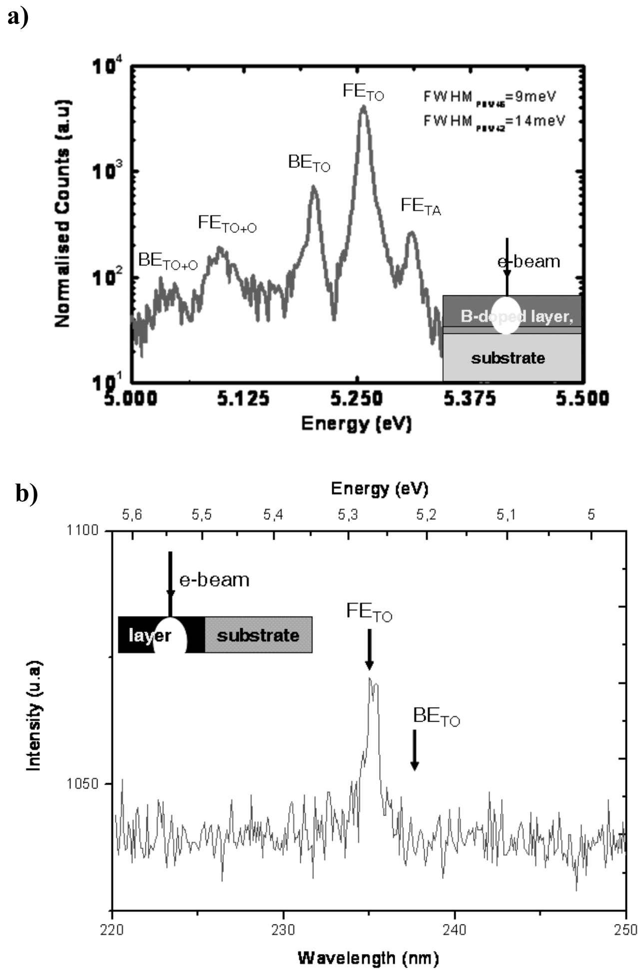

Figure 4 Helium temperature CL spectra recorded on sample B with a beam energy of 10 keV, (a) plan view electron excitation on the bulk sample (see inset for the geometry) in the excitonic emission range, (b) CL spectra recorded in cross sectional orientation (see inset) of the epilayer (location E in Fig. 3c).

Indeed, for heavy doping, the bound to acceptor peak (BE_{TO} , transition involving also an optical tranverse phonon replica) is reported to shift in energy depending on the boron doping level [5], while for lower doping (below 10^{19}cm^{-3}), this peak energy does not change and the ratio between free and bound exciton intensities can be used to determine doping level [4]. The latter work proposes the following empiric relation de deduce the boron doping at low temperature:

$$[B]=2.6 \times 10^{17}\ r \qquad (4)$$

where r is the ratio between BE_{TO} to FE_{TO} intensities at low temperatures. Such methodology can be also used to obtain the donors (phosphorus) doping level [10].

In Fig. 4, sample B CL spectra are shown in both plan view and cross section orientation respect to the electron beam. Figure 4a shows the excitonic recombinations with their different phonon replica usually observed on MPCVD diamond. From the BE_{TO} to FE_{TO} ratio, a doping level of 10^{16} cm^{-3} is deduced. However, at 10 keV beam energy some carrier recombination can occur below the 2 µm thick epilayer, which will reduce the BE_{TO} peak (see in the inset the white circle representing the volume of interaction between the high energetic incident electron and the diamond structure). Then, a FIB-dual beam lamella has been prepared to achieve cross section CL observations. The prepared lamella is 0.5 µm thick and the geometry of the experiment is shown in Fig. 4b inset. In the spectrum, the position of the BE_{TO} is indicated and the peak is below the noise intensity, which do not allow to verify the doping level.

The reason for such low CL emission intensity is obviously the reduced thickness of the lamella that limits e-h generation.

However, on this sample, much more intense peaks have been recorded, in the visible part of the spectrum, due to the presence of crystalline defects. Their respective transitions will then reduce excitonic recombinations weakening the corresponding peaks in Fig. 4b.

Figure 5 shows CL spectra recorded in plan view and cross section orientation. The location of the spectra recorded at 10 keV is indicated in Fig. 5c. It corresponds to a CTEM observation recorded on the [100] pole using the 220 reflection in dark field (DF) conditions. The micrograph shows that no doping related contrast can be observed and that no dislocations are here present. Indeed, those observations are recorded on the same lamella and same region respect to the Fig. 5b CL spectra: after the CL experiment the lamella was thinned down to 100 nm to allow the TEM observations. The location of the substrate-layer interface (dashed line) corresponds to the nominal value indicated by the growers as no contrasts are observed; however, the CL spectra seem to corroborate the location of the interface. The dark spots at the left hand side of the micrograph are Pt precipitates and the vertical lines correspond to thickness variations. Both are induced during the FIB preparation. In addition the white constrasts observed in the layer are also FIB-related preparation artefacts.

In Fig. 5b, thin lines at 3.188, 2.369, 2.154, 1.911 eV are observed in addition to the large band at 2.9 (A-band), 2.5 eV and 2.3 eV (green band). The 2.9 band is usually labelled A-band and indicates presence of dislocations or sp^2 bonds. In the present case this band is not present in the substrate or at the interface but increases in the epilayer. As no dislocations are observed by TEM, this band is here

© 2011 WILEY-VCH Verlag GmbH & Co. KGaA, Weinheim

attributed to sp^2. This behaviour is corroborated by the other peaks observed at 3.188 and 2.154 eV, usually observed on irradiated, ion implanted samples (labelled in some cases as T1 center) or at grain boundaries of polycrystalline diamond. It seems to be induced by complexes involving H and N atoms as for the NE3 center observed at 2.369 eV. This indicates that nitrogen and hydrogen have been incorporated during the CVD growth and also in the substrate [11].

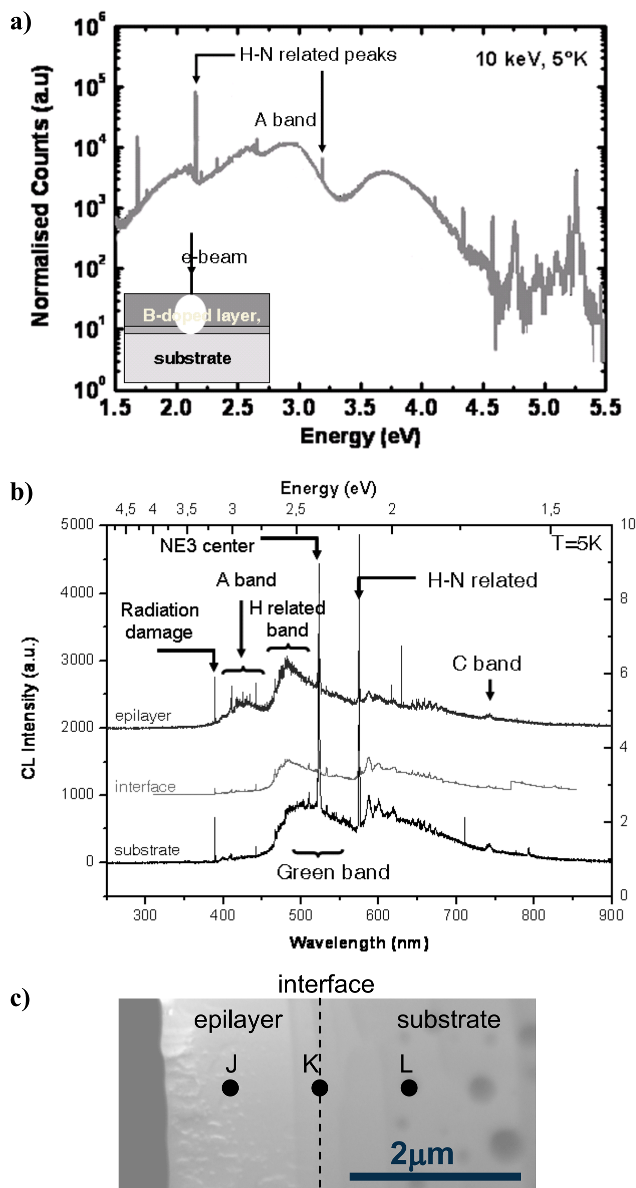

Figure 5 Helium temperature CL spectrum of sample B, (a) plan view electron excitation on the bulk sample (see inset for the geometry), (b) CL spectra recorded at different locations (layer: position J in Fig. 5c, interface: position K and substrate: position L) in cross sectional orientation, (c) CTEM micrograph of the same lamella after FIB thinning down to 100nm. The micrograph is recorded on 220 dark field conditions.

Finally, the C-band, that consists in a broad structured band, induced by the GR1 center, is also present in slightly boron doped material after irradiation or near dislocations. This means, in summary, that all those peaks correspond to point defects involving boron, hydrogen and some of them also nitrogen indicating that growth parameters could still be improved to optimized doping.

4 Conclusions A methodology to evaluate boron doping and defects presence in boron-doped homoepitaxial diamond layers is presented. This methodology is based in electron microscopy techniques. On one hand, analysis of the diffraction contrasts and the high angle annular dark field intensities reveal that both are suitable techniques to evaluate boron content in diamond epilayers when the dopant level is high, over the 10^{19} cm^{-3} scale. HAADF offers a better spatial resolution than DC, although numerical simulations are required to quantify boron content. When the boron level is below the mentioned scale, cathodoluminisce on cross section foils constitutes a more suitable methodology. The analysis of the spectra reveals the sp^2 bonds associated defects. As sharp as 5nm thick doping transition are shown to be grown and point defect involving boron and hydrogen atoms are shown to be present. sp^2 bonds are also observed in the epilayer.

Acknowledgements This work has been performed using the Electron Microscopy Facilities of the University of Cádiz (Spain). Authors thank the finantial support of the Ministerio de Ciencia e Innovación of Spain (MICINN) under the project TEC2009-11399.

References

[1] E. Kohn and A. Denisenko, Thin Solid Films **515**, 4333 (2007).

[2] R. S. Balmer, I. Friel, S. M. Woollard, C. J. H. Wort, G. A. Scarsbrook, S. E. Coe, H. El-Hajj, A. Kaiser, A. Denisenko, E. Kohn, and J. Isberg, Phil. Trans. R. Soc. A **366**, 251 (2008).

[3] T. Klein, P. Achatz, J. Kacmarcik, C. Macenat, F. Gustafsson, J. Marcus, E. Bustarret, J. Pernot, F. Omnès, BoE. Sernelius, C. Person, A. Ferreira da Silva, and C. Cyterman, Phys. Rev. B **75**, 165313 (2007).

[4] H. Kawarada, H. Matsuyama, Y. Yokota, T. Sogi, A. Yamaguchi, and A.Hiraki, Phys. Rev. B **47**, 3633 (1993).

[5] A. Deneuville, C. Baron, S. Ghodbane, and C. Agnès, Diam. Relat. Mater. **16**, 915 (2007).

[6] D. B. Williams and B. Carter, Transmission Electron Microscopy – A Textbook for Materials Science, Vol. II: Diffraction (Plenum Press, New York, 1996), p. 205.

[7] P. A. Doyle and P. S. Turner, Acta Cryst. A **24**, 390 (1968).

[8] M. Shiojiri and T. Yamazaki, J. Microsc. **223**, 172 (2006).

[9] D. Araújo, P. Achatz, R. El Bouayadi, A. J. García, M. P. Alegre, M. P. Villar, F. Jomard, and E. Bustarret, Diam. Relat. Mater. **19**, 972 (2010).

[10] J. Barjon, P. Desfonds, M. A. Pinault, T Kociniewski, F. Jomard, and J. Chevalier, J. Appl. Phys. **101**, 113701 (2007).

[11] A. M. Zaitsev, Optical Properties of Diamond: A Data Handbook (Springer, Berlin/Heidelberg, 2001).

© 2011 WILEY-VCH Verlag GmbH & Co. KGaA, Weinheim